PROCEEDINGS of the
23rd International Congress on Acoustics

9 to 13 September 2019 in Aachen, Germany

Investigation of the applicability of acoustic emission and vibration analysis to describe the thermo-mechanical mechanism during ultrasonic metal welding

Elie ABI RAAD[1]; Isabel BALZ[2]; Uwe REISGEN[2]; Michael VORLÄNDER[1]

[1] Institute of Technical Acoustics, Germany

[2] Welding and Joining Institute, Germany

ABSTRACT

Ultrasonic Metal welding (USMW) is particularly suitable for connecting electrotechnical components. Despite industrial spread, unexplainable process fluctuations may occur in USMW. This largely originates from the lack of profound scientific knowledge and understanding of the interdependency between tools and joining members. The aim of this research is to derive characteristic features, which correlate with the mechanisms during bond formation and joint properties, to achieve a more profound understanding, and in the future to open up new possibilities for online process control monitoring. In this study, copper sheets (CW008A) were ultrasonically welded at 20 kHz to study their effects on the thermo-mechanical mechanism during welding. Two laser vibrometers recorded the tool vibrations of the anvil and horn, directly connected to the sheets, and a ¼' microphone recorded the airborne sound. Additional T-peel tensile testing and laser scanning microscopy of the fractured surface at different welding stages are used for validation. The results of this paper provide a more profound understanding of the thermo-mechanical mechanism during USMW and will introduce a prospective improvement in quality and process stability.

Keywords: vibroacoustics, ultrasonic metal welding, bond formation

1. INTRODUCTION

Ultrasonic metal welding (USMW) is a solid state welding process that uses high frequency oscillations and a static clamping force. It is widely used in various industry applications such as joining in electric motors, strand welding in harness production or in the assembly and connection of battery cells (1). Since bonding is formed in solid state, common geometric and metallurgical problems encountered in fusion welding of aluminum and copper, such as gas porosity, intermetallics and embrittlement (2) are avoided. Further reasons for the industrial widespread of USMW are its low energy consumption, the short welding times and its good automation capacity. Although there is extensive research on the bond formation in USMW, there is still a lack of profound understanding of the thermo-mechanical mechanism during welding, which is essential for weld optimization.

In USMW, various binding mechanisms have been proposed such as mechanical interlocking, melting, adhesion, recrystallization and even diffusion (1, 3, 4) whereby in the last studies (4, 5) mainly dynamic recrystallization (DRX) is regarded as the primary binding mechanism. The bond formation is described by different process stage models. There is agreement that periodic shear deformations at the interfaces are significantly responsible for the bond formation in USMW (5). The temperature increase with increasing welding time is caused by friction and deformation (5). The friction conditions and the development of plastic deformations are strongly influenced by welding parameters (7, 8). Thus, friction work increases with increasing oscillation amplitude and is in non-linear relation to the welding pressure (6, 7, 9). According to (5, 6, 10), friction energy dominates the initial welding process and is mainly responsible for the breaking of oxides and surface cleaning. As welding time increases, the temperature of the joining members rises and results in material softening (5, 6). This leads to a larger plastic deformation and favors the bond formation. Theoretical and experimental analyses (6, 11) have shown that a thermal-stationary stage is established at the end of welding in which no further plastic deformation occurs and the maximum bonding area is achieved.

[1] elie.abiraad@akustik.rwth-aachen.de

There are different theories regarding the description of an ideal end of process. Some researchers (4, 6) describe a stagnation of the joint strength, whereby others (8, 11) observe a decrease in the joint strength exceeding a critical welding time or welding energy. This decrease in strength is explained by material fatigue (8, 11). Other studies (9) observe a slip between the horn and the upper joining member during over-welding, whereby tool sticking reduces the final joint strength. Other authors (3, 5) describe over-welding as a breakage of previously bonded regions by further oscillating excitation.

In-situ measurement during USMW as a highly dynamic process is still challenging. Therefore, most of USMW research results are based on post-weld characterizations. As a result, there are barely any direct observations about bond formation, which are essential for a fundamental understanding.

Laser Doppler Vibrometer (LDV) measurement of single spot (12) or multiple spots (5) was used to determine the oscillations during USMW. Lu et al. (5) used a Photonic Doppler Velocimetry (PVD) system to study the relative motion between the horn, aluminum foils and anvil. It was shown that the welding process consists of four different welding stages: The first two stages - slip [1] and slip-stick [2] - are characterized by a large relative motion between both foils [1] and between horn and upper foil [2] which are essential to disperse oxides and contaminations as well as to increase frictional heat. The stick stage [3] is mentioned as the key stage where bond development and DRX increase with welding time. The maximum strength is obtained when horn and foils oscillate with similar velocity. Over-welding [4] is characterized by a quick drop in bottom and top foil velocities which can be caused by tool sticking or breakage of previously bonded regions.

The above-mentioned studies have shown initial results on relative motions of the tools and the joining members during USMW. However, there is still a lack of characteristic variables from sensor signals, which correlate with the mechanism during bond formation and introduce the prospective to apply monitoring criteria for USMW.

In this paper, acoustic emissions and characteristic vibrations of the horn and anvil produced during welding are measured to study their relationship to bond formation in ultrasonic welding and to joint quality. Acoustic emissions have already proved useful for tool condition monitoring and online process control (13, 14). This is possible because friction produces acoustic emissions characteristic of the condition of the surfaces in friction (15, 16, 17). As for the vibrations, they should take into account mode coupling, in which different tools with different modal behaviors affect each other's vibrational patterns (15). In our case, this means that each of the horn and anvil, when coupled during the welding process, will behave differently than they would if they were vibrating alone.

2. EXPERIMENTAL SETUP

2.1 Metrological test setup for acoustic emission and vibration monitoring

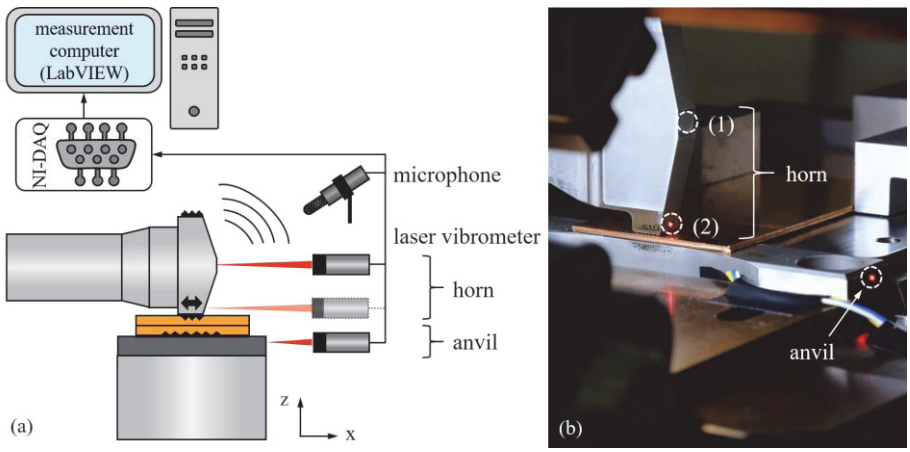

Figure 1 – (a) Schematic illustration of measurement setup and (b) zoomed-in view showing the measuring positions on horn and anvil during copper sheet welding

In this study two Compact Laser Vibrometer "CLV-2534" from Polytec and a ¼' GRAS microphone were used to record the vibrations of the horn and the anvil along the welding direction and the airborne emissions during welding. Data from all three of those sensors was synchronously recorded at a sampling rate of 250 kHz. The microphone was placed 50 cm away from the joining area and directed towards it. Both LDV use a 633 nm wavelength helium-neon-source. The locations of the

laser spots are illustrated in Figure 1. Despite the small spot size (~ 110 µm), measurement errors due to process emissions, such as metal particles and dust, increasingly dominated at the measurement position 2, close to the weld zone. Therefore, the majority of the experimental measurements were carried out in the middle of the horn (position 1).

In order to estimate the temperature development during bond formation, two K-type thermocouples (Ø 0.51 mm) were ultrasonically welded at the top of the upper specimen at 10 mm (TC 2) and 17 mm distance (TC 3) from the horn. A third K-type thermocouple (Ø 0.13 mm) was placed between the two sheets in the middle of the welding zone (TC 1), as shown on Figure 2. The temperature measurements were carried out three times for over-welding and in addition to the main experiments.

2.2 Ultrasonic welding setup

For the investigation, similar lap welds made of copper (CW-008A, R240) sheets with 0.8 mm thickness were prepared by USMW. The dimensions of the samples were 45 mm x 125 mm. The rolling direction (RD) of the sheets was in the oscillation direction (OD) as shown in Figure 2. A Schunk Sonosytems LS-C longitudinal welding system with a 20 kHz operating frequency and a maximum power of 4 kW was used for welding. The maximum vibration amplitude under no-load conditions was 28 µm. The dimension of the horn surface was 8 mm x 8 mm knurled with 0.8 mm base side, 0.3 mm height and 90° apex angle. In order to reduce inconsistency in weld quality, energy-controlled mode was mainly used in the present study. The welding parameter were set based on preliminary experimental tests. The maximum joint strength can be achieved with a clamping force of 2250 N ($p_{cylinder}$ = 4.5 bar), an oscillation amplitude of 26 µm (≙100%) and a weld energy of 1800 Ws (~870 ms). In order to be able to analyze the effects of over-welding as well, the welding tests were carried out with an increased weld energy of 2100 Ws (~1030 ms). In addition, the welding process was interrupted every 50 ms for sampling to evaluate the bond formation.

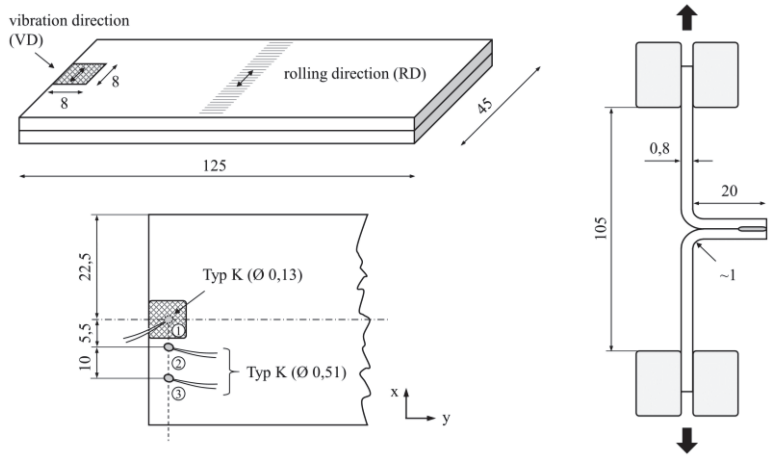

Figure 2 – Geometric specifications of weld specimen

2.3 Evaluation of the bond

T-peel tensile testing based on DIN EN 14270 as shown in Figure 2 was performed to evaluate weld quality and to observe the fractured surface. After welding, the sheets were bent by 90° in two directions to allow the specimen to be clamped. A load was then applied to peel the weld sample with a displacement rate of 10 mm/min. The maximum T-peel load from the load-displacement curve and the failure mode was recorded. For each investigated weld time, 3 replicates were evaluated.

In order to analyze the welded area (microwelds) with increasing welding time, the fracture surfaces of the peeled samples were measured with a laser confocal microscope “VK-X100” (Keyence) at 10x magnification. Furthermore the microscope was used to determine the penetration depth of the horn (5x magnification) at different welding times.

3. EXPERIMENTAL RESULTS

3.1 Joint strength and weld formation

As the maximum peel forces are good indicators for bond formation, they are plotted as a function of welding time in Figure 3. First, the joint strength increases with weld time and interfacial failure

("cold weld") is observed for welding times lower than about 0.5 s. Within this welding time range, the fracture surface (see Figure 4) changes from a few scratch marks within the first 150 ms to extensive plastically deformed and bonded areas with increasing weld time. At welding times between 0.5 ms to 0.7 ms the fracture mode changes and interfacial separation with scattered tear inside the welding zone can be observed. At the same time the joint strength stagnates in this time range. With increasing welding time up to 0.9 ms the breaking forces but also the variance rise by reaching the highest bonding area. With further welding time the joint strength decrease ("over-weld"). Here a nugget pull-out fracture can be observed due to thinning and breakage of welding specimens by excessive plastic deformation.

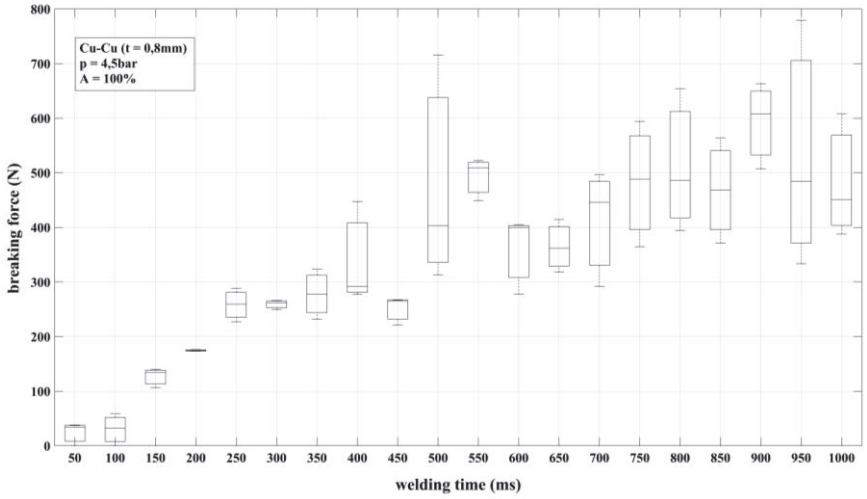

Figure 3 – Maximum peel load as a function of welding time

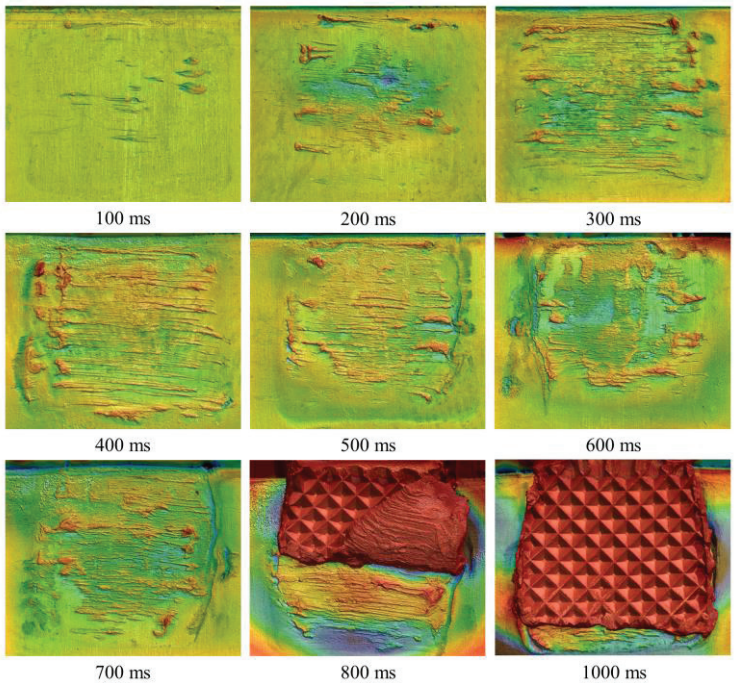

Figure 4 – Fracture surfaces measured with laser confocal microscope for different welding times

Figure 5 (a) shows an exemplary temperature curve during a typical over-welding process at different thermocouple positions. The temperatures within the welding zone (TC 1) rise very strongly at the beginning of the welding process until the temperature rise slows down at ~0.2 s. At 0.6 s a further temperature rise is visible, which causes the joining temperature to rise to the maximum of 500°C by the end of the welding process. The other measuring positions on the upper sheet show a similar curve, but reach maximum temperatures of 280°C (TC 2) and 230°C (TC 3) respectively.

The penetration depth of the horn during over-welding can be determine by the vertical

displacement of the horn given by the welding system as well as by measuring the horn imprints on the surface of the upper sheet after different welding times. For comparison, the determined penetration depth curves from the two methods can be seen in Figure 5 (b). Both curves show a similar trend: in the initial stage of the welding process (< 0.15 s) there is a large material compaction, between 0.15 s - 0.6 s the compaction rate slows down and increases again at 0.6 s.

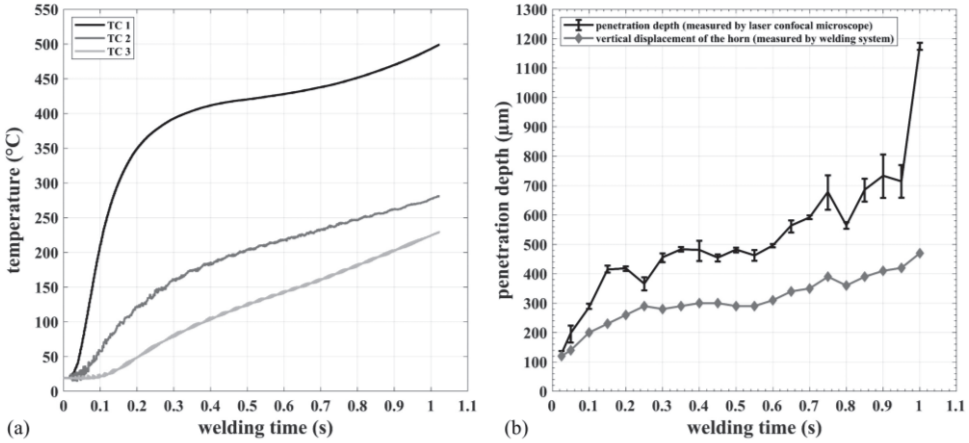

Figure 5 – (a) Temperature development and (b) penetration depth of the horn during over-welding

3.2 Vibroacoustic results

The following figures describe the behavior of the horn and anvil, as well as the sound received by the microphone, during both a free run and during a typical welding. A free run is defined as having the horn vibrating alone, without any connection to the anvil or to metal sheets. The laser vibrometers were found to be sensitive to vibrations from the environment such as passing cars and other machines operating nearby. The data was therefore filtered using a high-pass filter with a 1 kHz cutoff frequency. In addition, since the vibrometers measure the velocity of vibration of a surface, the data was then integrated once to get the vibrations of the horn and anvil surfaces in time.

Figure 6 shows spectrograms of the acoustic emissions recorded by the microphone and the vibrations of the horn during a free run. As can be seen, the airborne sound and the horn vibrations contain more than one frequency. For the microphone, the pressure is concentrated in bands centered around harmonics of the welding frequency, 20 kHz, as well as harmonics of 10 kHz. For the horn, the vibrations are centered around 20 kHz and its harmonics. The anvil vibrations are not shown since, during a free run, the anvil is not excited by the horn and thus does not vibrate.

Figure 7 shows spectrograms of the airborne sound and horn during welding. Looking at the horn spectrogram, we can see the same frequency bands as during free run. However, the amplitude at 20kHz is smaller and the amplitudes of the other frequency bands are larger than during free run.

Figure 8, Figure 9 and Figure 10 show time plots of the airborne sound and the horn and anvil vibrations filtered in different frequency bands. Time plots were chosen instead of spectrograms to better show the amplitude variations of different frequency bands in time. The frequency bands were 10 kHz wide and centered on the first four harmonics of the welding frequency.

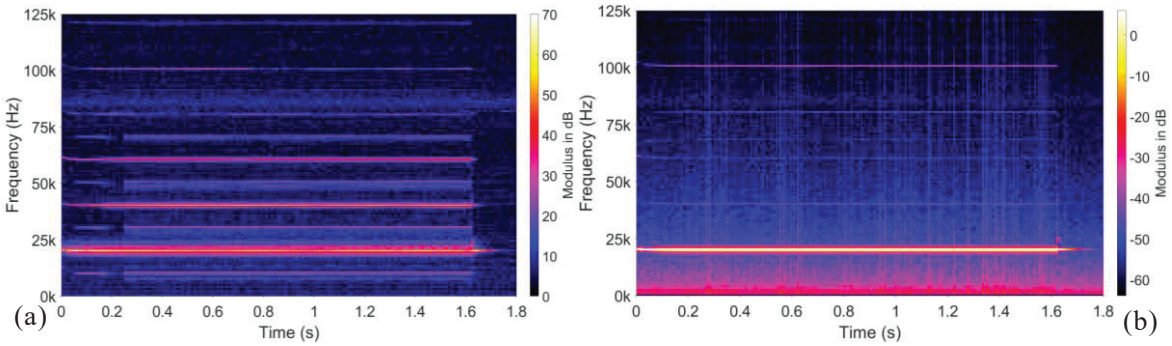

Figure 6– Spectrograms of (a) airborne sound and (b) horn displacement during free run

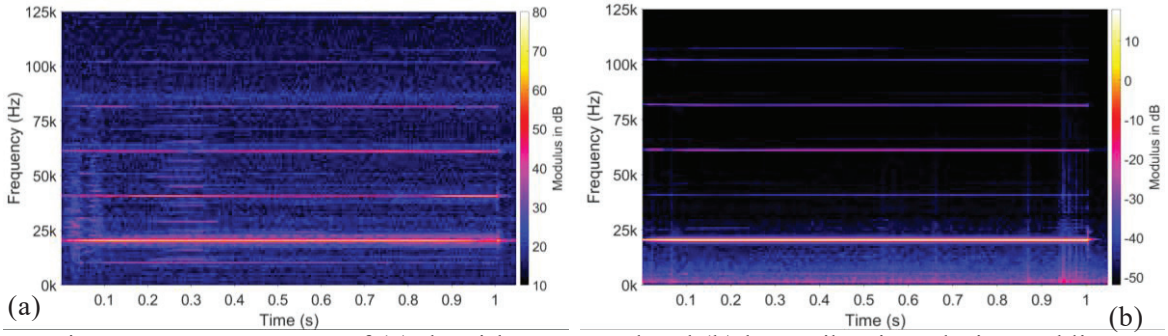

Figure 7– Spectrograms of (a) the airborne sound and (b) horn vibrations during welding

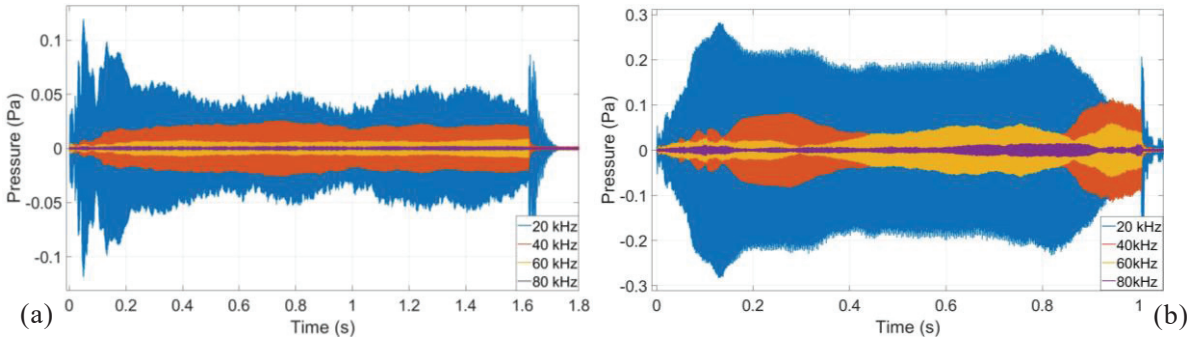

Figure 8- Amplitude of airborne sound during (a) free run and (b) welding

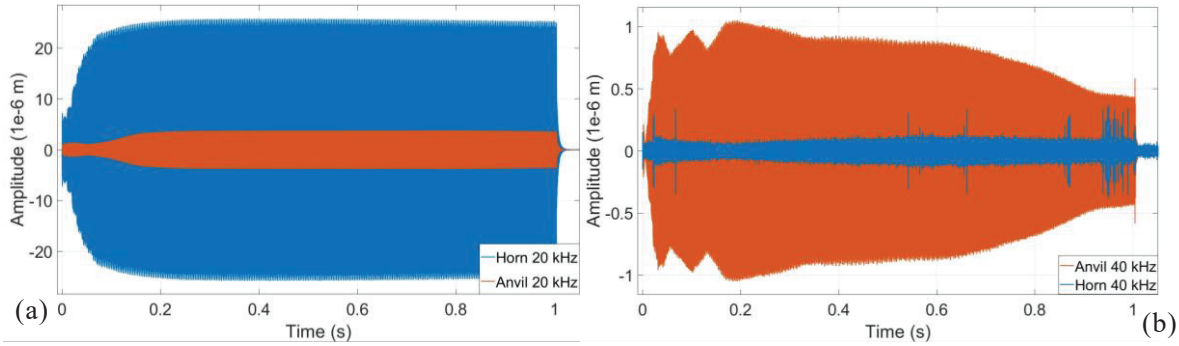

Figure 9- Amplitude of horn and anvil vibrations at (a) 20 kHz and (b) 40 kHz

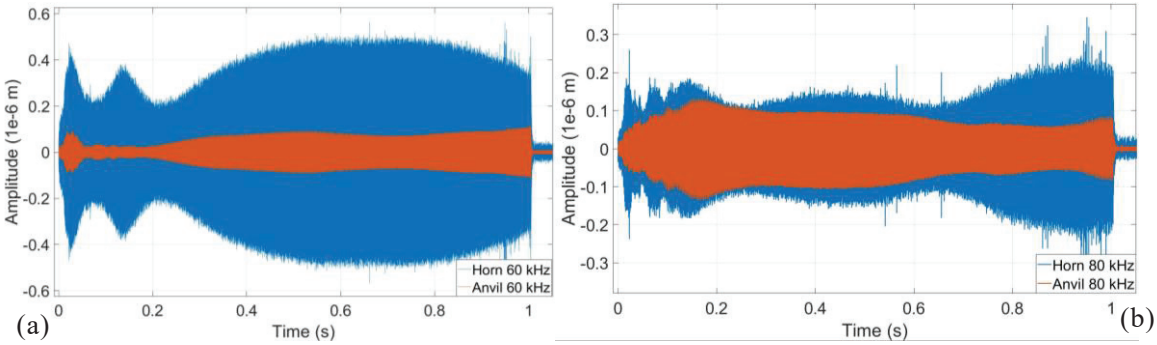

Figure 10- Amplitude of horn and anvil vibrations at (a) 60 kHz and (b) 80 kHz

4. DISCUSSION

The spectrograms show that the vibrations of the horn and the sound emissions during free run are mostly constant and distributed into multiple frequency bands. Hypothetically, different stages of welding would act as different boundary conditions between the metal sheets, since the bond strength between the metal sheets would be different, leading to different frequency contents in the acoustic emissions in the process. However, since the free vibrations of the horn, the source of vibrations in the welding process, already contain many frequency bands, finding the different welding frequencies becomes more complicated: one must now separate the frequencies produced by the different stages

of welding and the input frequencies. Though the anvil and horn would couple and affect each other's modal response during welding, it is not clear exactly how, and the possibility of a frequency coming from the horn rather than from the welding process cannot be neglected. In addition, the vibrational measurements do not take into account the modal behavior of the horn and anvil at the point of measurement, which would explain the very low amplitudes for the horn vibrations at 40 kHz.

Based on the findings from this study, the initial stage of the welding process (< 0.2s) is a coupling stage in which the welding tools and the metal sheets connect better. There is a large increase in vibrations in the horn and anvil at the welding frequency, with the horn vibrations increasing before the anvil vibrations, and with a steeper slope. This increase in vibration leads to the increase in temperature, due to an increase in friction work between the horn, the sheets, and the anvil. This is also confirmed by the low joint strengths and the observed scratch marks on the fracture surfaces. The rising temperatures lead to a softening of the copper, favoring the horn penetration into the material, thus the knurls of the horn completely plunged into the upper sheet at the end of this initial stage. This stage continues until approximately 0.2s, at which point the anvil and horn reach a sort of steady state of the vibrations at 20 kHz.

The better coupling between the horn and the upper specimen causes lower overall friction work and thus slows the temperature rise down. Therefore the breaking forces stagnate at a first joint strength level (~ 260 N) as well as the penetration depth of the horn in a time range from 0.2s to 0.5s. For the vibrations, there is an increase of the horn vibrations at 40, 60 and 80 kHz, a decrease of anvil vibrations at 40 kHz, and an increase of anvil vibrations at 60 and 80 kHz. This could indicate slipping between the bottom sheet and the anvil at 40 kHz.

The increasing plastic deformation within the welding time range of 0.5s to 0.7s, identifiable by the further penetration of the horn, leads to a further growth of the bonded area and to a second joint strength level (~ 400 N), in which in addition to the previously observed adhesive failure, interfacial separation with scattered tear may occur. In accordance with the findings from previous study (6), friction heat is reduced with increasing material softening, causing temperatures to stagnate slightly. Meanwhile, the horn vibrations and the anvil vibrations at 20 kHz do not change much. At 40, 60 and 80 kHz, the anvil vibrations decrease, with an inflection point around 0.7s. The decrease in anvil vibrations could indicate slipping somewhere between the horn and the anvil. At this stage, it is most likely to be slipping between the bottom sheet and the anvil.

Significant material softening occurs after approximately 0.7s, which leads to a typical bending of the upper sheet around the heat affected zone. The additional deformation work is considered as a cause of the renewed temperature rise. This comes with a decrease in the horn vibrations at 20, 40 and 60 kHz and in the anvil vibrations at 20, 40 and 80 kHz, as well as an increase in horn vibrations at 80 kHz and in anvil vibrations at 60 kHz. These changes can be seen as a continuation of the state of vibrations in the previous phase: further increase in the bonding area leads to a better coupling of the metal sheets, which helps in getting a better coupling of the horn and anvil, and leads to further decreases in the amplitude of vibrations of the anvil and horn. This is different from the initial stage, when better coupling meant higher vibration amplitudes of the anvil. In the beginning, a better coupling leads to better excitation of the anvil, but for a very strong coupling, the horn would carry so much of the mass of the anvil that the vibrations of the horn would decrease in amplitude.

At a welding time of 0.9s the largest bonding areas are reached, and the maximum breaking forces (~ 600 N) can be observed. There is also an inflection point in the plots of the vibrations of the horn and anvil in all frequencies.

If welding time exceeds approximately 0.9 s the specimens are thermally and mechanically overstrained ("over-weld"). Temperatures and penetration depth of the horn reach their highest levels resulting in nugget pull-out failure and a reduction in joint strength due to excessive plastic deformation of the upper sheet. This is accompanied by noticeable changes in the vibrations of the anvil, with a strong increase at 60 and 80 kHz and a slowing down of the decrease at 40 kHz. This indicates an increase of the vibrations received by the anvil at those frequencies. This could be due to the fatigue failure of microwelds in the overwelding stage, which would release high-frequency vibrations into the anvil.

The sound pressure was not used much in this discussion, as its inflection points do not correlate with the results from the other sensors. This could be due to the presence of at least one other sound source in the room other than the vibrations of the horn, anvil, and copper sheets. Further research is required before using the airborne sound.

5. CONCLUSIONS

During ultrasonic metal welding, the interaction between the anvil and the horn is complex, and greatly depends on the transfer of vibration from the horn, to the top sheet, to the bottom sheet, and finally to the anvil. These connections depend on the type of frictional coupling between each element, as well as the state of the weld between the two sheets. In this paper, we have tried to find features to describe the different stages of the welding process by looking at data recorded by various sensors during welding and by post-weld testing. Correlations between the temperature, the vibrations of the tools, the penetration depth, the bond strength and the bond area could be found at different points in time, and were linked to the different stages of welding. However, some elements of vibrational behavior and the airborne sound could not be properly explained yet.

ACKNOWLEDGEMENTS

The authors would like to thank the German Research Foundation DFG for the support of the research work under grant number RE2755/52-1. For the sponsorship and the support, we wish to express our sincere gratitude.

REFERENCES

1. Wodara J, Herhold H. Ultraschallfügen und -trennen: Band 1 der Grundlagen der Fügetechnik. DVS Verlag (Fachbuchreihe Schweißtechnik 151). Düsseldorf, Germany 2004.
2. Adam T. Ultraschallschweißen ausgewählter Aluminiumlegierungen mit erhöhter Festigkeit. Otto-von-Guericke-Universität Magdeburg, Institut für Füge- und Strahltechnik. Dissertation. Magdeburg, Germany 1999.
3. Harthoorn JL. Ultrasonic metal welding. Technische Hogeschool Eindhoven. Dissertation. Eindhoven, Netherlands 1978.
4. Fujiia HT, Goto Y, Sato YS, Kokawa H. Microstructural evolution in dissimilar joint of Al alloy and Cu during ultrasonic welding. In: Materials Science Forum 783-786. 2014. p. 2747–2752.
5. Lu Y, Song H, Taber GA, Foster DR, Daehn GS, Zhang W. In-situ measurement of relative motion during ultrasonic spot welding of aluminum alloy using Photonic Doppler Velocimetry. In: Journal of Materials Processing Technology 231. 2016. p. 431–440.
6. Zhang C. A Thermomechanical analysis of an ultrasonic bonding mechanism. Utah State University. Dissertation. Logan, United States 2011.
7. Siddiq A, Ghassemieh E. Theoretical and FE analysis of ultrasonic welding of aluminum alloy 3003. In: Transactions of the ASME, Journal of Manufacturing Science and Engineering 131(4). 2009. p. 041007/1-11.
8. Kim W, Argento A, Grima A, Scholl D, Ward S. Thermo-mechanical analysis of frictional heating in ultrasonic spot welding of aluminium plates. In: Proceedings of the Institution of Mechanical Engineers. Part B (Journal of Engineering Manufacture) 225 (7). 2011. p. 1093–1103.
9. Satpathy MP, Moharana BR, Dewangan S, Sahoo SK. Modeling and optimization of ultrasonic metal welding on dissimilar sheets using fuzzy based genetic algorithm approach. In: Engineering Science and Technology, an International Journal 18 (4). 2015. p. 634–647.
10. Siddiq A, Ghassemieh E. Thermomechanical analyses of ultrasonic welding process using thermal and acoustic softening effects. In: Mechanics of Materials 40 (12). 2008. p. 982–1000.
11. Chen KK, Zhang YS, Wang HZ. Study of plastic deformation and interface friction process for ultrasonic welding. In: Science and Technology of Welding and Joining 22 (3). 2016. p. 208–216.
12. Balle F, Wagner G, Eifler D. Charakterisierung des Ultraschallschweißprozesses durch hochauflösende Laser-Doppler-Vibrometrie. In: InFocus – Magazin für Optische Messsysteme (1) 2009.
13. Martins H R C, Aguiar P R, Frech A Jr, Bianchi E C. Tool condition monitoring of single-point dresser using acoustic emission and neural networks models. IEEE Transactions on Instrumentation and Measurement 2014; 63(3)
14. Ding N., Zhao C, Luo X, Shi J. An Intelligent Grinding Wheel Wear Monitoring System Based on Acoustic Emission. Solid State Phenomena 2017;261 p.195-200
15. Kragelskii I V. Friction and Wear
16. Akay A. Acoustics of friction. The Journal of the Acoustical Society of America 2002; 111(4)
17. Thompson D J. On the relationship between wheel and rail surface roughness and rolling noise. Journal of Sound and Vibration 1996; 193(1):149-160